Locomotion of Pulse-Driven Microcapsule Robot on Inclined Plane

Phunopas A.
Faculty of Computer Science and Systems Engineering, Kyushu Institute of Technology, Fukuoka, Japan

Ito T., Kito Y.
Faculty of Computer Science and Systems Engineering, Kyushu Institute of Technology, Fukuoka, Japan

Ishimori S.
Faculty of Computer Science and Systems Engineering, Kyushu Institute of Technology, Fukuoka, Japan

Hayashi T.
Ogasawara Precision Laboratory, Kanagawa, Japan

Abstract
We have developed a microcapsule robot that has a smooth outer surface and is driven by inertia and friction forces. There are no protrusions to harm the soft tissue of the intestines. The microcapsule robot consists of the body mass and the inner mass. The motion of the inner mass is generated by an inducing coil. This paper describes the investigation and analysis of the microcapsule robot motion on an inclined plane. Displacement of the microcapsule robot was measured by a high-speed camera. The experimental results demonstrate that the microcapsule robot can move upwards on an inclined plane at a small angle between 0 and 15° and consumes only 4 volts. This device is advantageous for medical purposes such as drug delivery, disease diagnosis and teleoperated surgical robots.

Keywords*: Capsule robot, Micro-mechanism, Magnetic drive*

1 Introduction

Many types of capsule robots have been fabricated as drug delivery systems in the last 40 years[1]. Most of them, however, do not have a driving mechanism and are simply a means of first-period drug delivery. Although the human digestive system is able to drive capsule robots along with ingested foods, self-motion capability is necessary for advanced applications such as delivery of medicine to a targeted position, disease diagnosis and teleoperated procedures. All advanced applications rely on tools that are installed on capsule robots. Capsule endoscopy with an installed compact camera is one example of an advanced application presently used in this field[2], and constitutes important progress for medical treatment because the patient needs only to swallow a smart capsule robot. This is similar to taking normal medicine except that the smart capsule robot can travel through the human alimentary canal. Recent developments have produced several different types of capsule robot driving mechanisms, such as the screw mechanism[3], multilegged mechanism[4], inchworm mechanism[5] and electrical stimulus[6], which are able to generate motion. However, there is a risk of damage to the soft intestinal tissue by protrusions and severe grazing by the capsule robot. We have therefore developed a travelling capsule robot that has a smooth surface and is driven by inertia and friction forces. We also propose an image processing method to measure the capsule robot motion by high-speed camera. This paper begins by explaining the structure of the capsule robot, the pattern of motion of the capsule robot and the mathematical model. The next section covers the capsule robot operation. The experiment section describes the limitations of motion related to the coefficient of static friction. Then, the simulation

results are presented. The simulation tool allows us to predict the trends in capsule robot velocity on the inclined plane.

2 Principle of motion

2.1 *Capsule robot structure*

A capsule robot comprises three main parts: a body mass, an inner mass and a coil, as shown in Figure 1. The inner mass is an Nd-Fe-B permanent magnet driven by electromagnetic force generated by the inducing coil. The parameters of the capsule robot are shown in Table 1. The coil is made by turns of Ø 0.2 mm copper. The inner mass is smaller than the body mass and moves back and forth inside the body mass. The stroke length is therefore limited by the length of the body mass. For the theoretical analysis, the motion of the capsule robot was divided into four steps by behavior and moving direction.

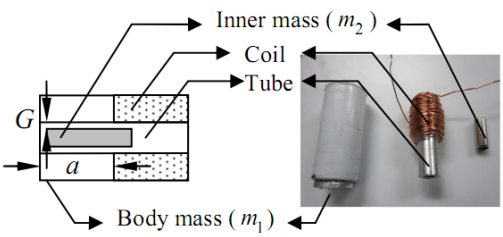

Figure 1: Main parts of the capsule robot

Table 1: Parameters of the capsule robot

Part	Mass (g)	Size
Inner mass	0.05	Ø 1.5 mm × 9 mm
Body mass	1.45	Ø 7 mm × 16 mm

The direction of electromagnetic force, friction force, velocity of the body mass and velocity of the inner mass are shown in Figure 2. The capsule robot changes from one step to another by collision. After the collision, the electromagnetic force is reversed by inverting the direction of the current to the coil. These are the characteristics of one period of motion.

Step 1: Electromagnetic force pushes the inner mass with velocity while the body mass is inversely moving with velocity against the friction force.

Step 2: After the inner mass is accelerated, it approaches the body mass until a collision occurs. The body mass and the inner mass move together with the same velocity, and are decelerated by friction force.

Step 3: This is similar to Step 1 except that it changes the electromagnetic force direction by inverting the step shape current to the coil. The electromagnetic force then becomes. The inner mass moves with velocity while the body mass is inversely moving with velocity against the friction force.

Step 4: After the collision, the body mass and the inner mass move together with the same velocity, and are decelerated by friction force in a similar manner to Step 2. The displacement of each set of four steps is combined to give the total distance.

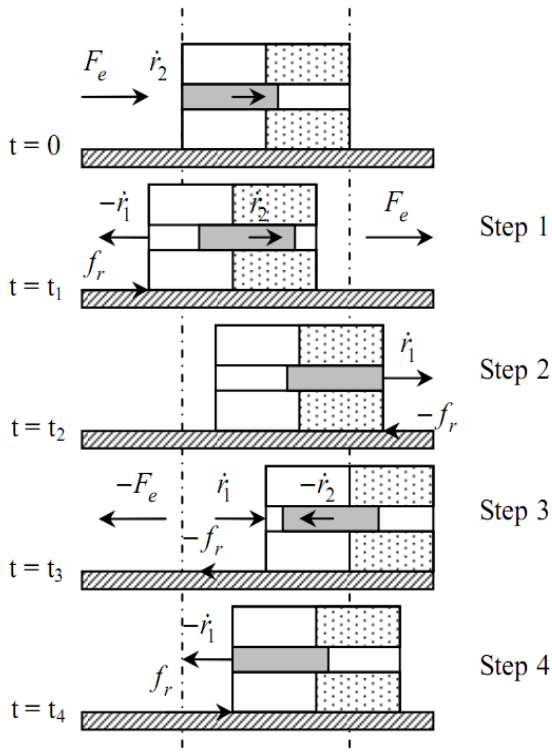

Figure 2: Four steps of capsule robot motion

2.2 *Capsule robot structure*

The equations of motion are derived using the inclined plane as shown in Figure 3. There are two subsystems: mechanical and electrical. The mechanical subsystem is given by Equations (1) and (2). Friction force changes direction depending on the direction of as Equation (3). The total mass is calculated by Equation (4). However, we disregard the friction force between the inner mass and the body mass for the sake of simplification. The capsule

robot moves in a forward and backward direction. The global framework is defined by the x-y Cartesian coordinates shown in Equation (5).

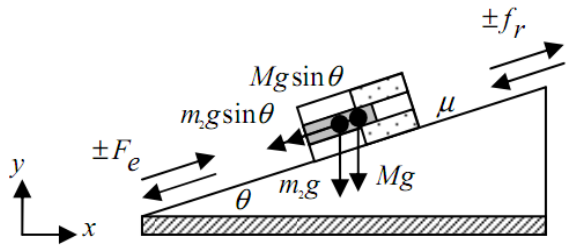

Figure 3: Free-body diagram of the capsule robot on an inclined plane

$$-F_e = m_1\ddot{r}_1 + Mg\sin\theta + f_r \quad (1)$$

$$F_e = m_2\ddot{r}_2 + m_2 g\sin\theta \quad (2)$$

$$f_r = sign(\dot{r}_1)\mu Mg\cos\theta \quad (3)$$

$$M = m_1 + m_2 \quad (4)$$

$$r_j^2 = x_j^2 + y_j^2 \qquad ; j = 1,2 \quad (5)$$

where

μ is the coefficient of static friction

θ is the angle of the inclined plane

j is the mass number

The characteristics graph of the mechanical subsystem capsule robot as shown in Figure 4 is obtained from the equations of motion for the four steps of motion[7].

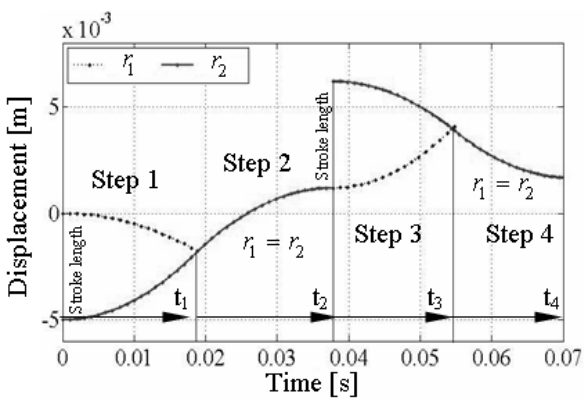

Figure 4: Motion characteristics of the capsule robot

The change from Step 1 to Step 2 and from Step 3 to Step 4 occurs when r_1 and r_2 intercept each other ($r_1 = r_2$). We assume that the collision is inelastic. Hence, the initial velocity v_0 is expressed as follows:

$$v_0 = \left(\frac{m_2\dot{r}_2 + m_1\dot{r}_1}{M}\right) \quad (6)$$

After the collision, the velocity of the body mass decreases until $\dot{r}_1 = 0$, where it will stop. Integrating Equation (1) ($F_e = 0$) yields the velocity and displacement of the body mass as in Equations (7) and (8). However, changing from Step 2 to Step 3 depends on the change in input voltage U.

$$\dot{r}_1 = v_0 - \left(g\sin\theta + \frac{f_r}{M}\right)\cdot t \quad (7)$$

$$r_1 = v_0 t - \left(g\sin\theta + \frac{f_r}{M}\right)\cdot\frac{t^2}{2} \quad (8)$$

The electrical subsystem is described by Kirchhoff's Voltage Law[8]. Electrical current i flowing through the coil generates electromagnetic force. The simple circuit consists of the linear displacement of the inner mass r_2, inductance of the coil L, resistance of the coil R, electromagnet current i and supply voltage of the coil U as shown in Figure 5. The equation for the electrical circuit is expressed as follows:

$$U = R.i + \frac{d}{dt}[L(r_2).i] \quad (9)$$

Transforming Equation (9) gives:

$$\frac{di}{dt} = \frac{1}{L(r_2)}\cdot\left[U - R.i - i\cdot\frac{dL(r_2)}{dr_2}\cdot\frac{dr_2}{dt}\right] \quad (10)$$

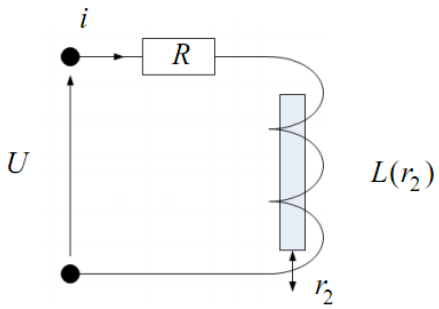

Figure 5: Equivalent diagram of the electrical circuit of the electrical subsystem

The magnetic system is assumed to be linear. The energy in Equation (11) is differentiated by r_2 to give the electromagnetic force in Equation (12).

$$W = \frac{1}{2} \cdot L(r_2) \cdot i^2 \tag{11}$$

$$F_e = \frac{1}{2} \cdot i^2 \cdot \frac{dL(r_2)}{dr_2} \tag{12}$$

Inductance of the coil is derived from reluctance $\Re_M$ of the system in Equation (13) where μ_0 is the permeability of space $4\pi \times 10^{-7}$ H/m, a is the gap length without the coil 8×10^{-3} m, d is the diameter of the tube 1.5×10^{-3} m, N is the number of turns of the coil and G is the gap between the inner mass and the tube of approximately 2×10^{-5} m.

$$\Re_M = \frac{G}{\mu_0 \cdot \pi \cdot r_2 \cdot d} + \frac{G}{\mu_0 \cdot \pi \cdot a \cdot d} \tag{13}$$

The magnetizing inductance is

$$L(r_2) = \frac{N^2}{\Re_M} \tag{14}$$

Substituting Equation (14) into Equation (12) gives the electromagnetic force:

$$F_e = \frac{i^2}{2} \cdot \frac{\mu_0 \pi a d N^2}{G} \cdot \frac{a}{(a+r_2)^2} \tag{15}$$

Consequently, the mechanical and electrical subsystems are combined. The system diagram is represented in Figure 6 using MATLAB Simulink. However, the simulation is an ideal case without collision. The equations are solved by numerical ode45 (Dormand-Prince). The results from simulation are shown in Section 5.

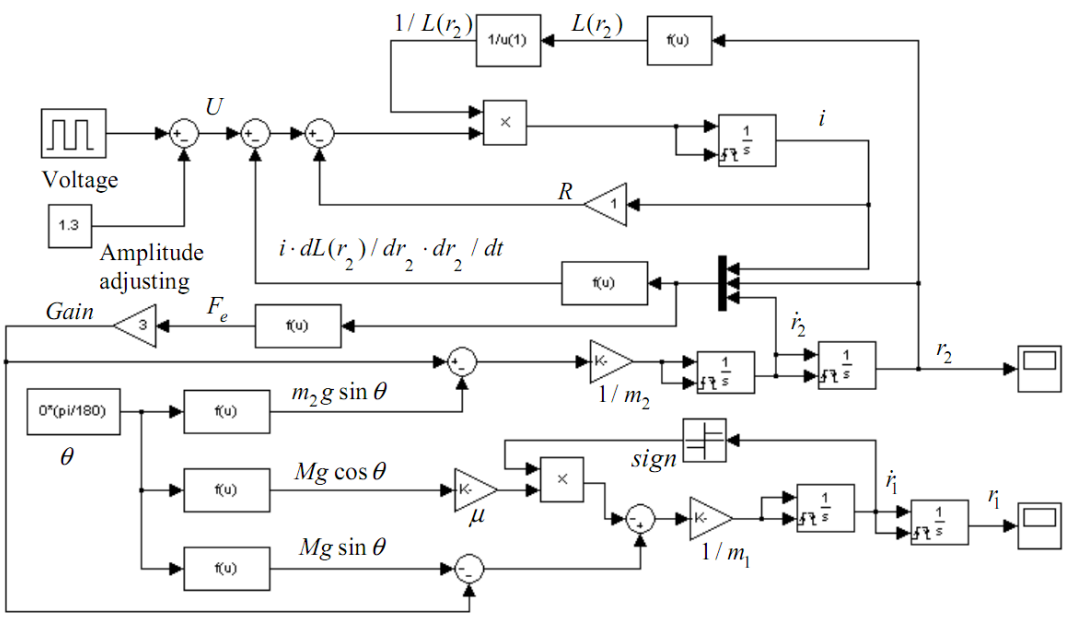

Figure 6: Diagram of the mechanical and electrical subsystems using MATLAB Simulink simulation

3 Capsule robot operation

3.1 Pulse induction

The input signal is PWM (pulse width modulation). The PWM signals are transmitted from the function generator to the induction coil. There are two patterns of control input for forward motion and backward motion of the capsule robot as shown in Figure 7. The positive and negative amplitude changes the direction of the current flow and flux in the coil, which prompts the inner mass to move back and forth inside the tube as shown in Figure 8. When the positive amplitude is greater than the negative amplitude, the robot moves forward, and when the opposite is true it moves backward.

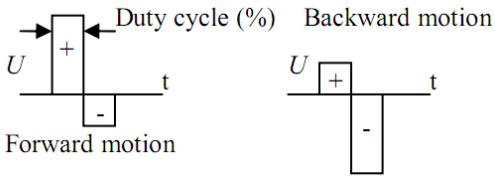

Figure 7: Control input of the capsule robot

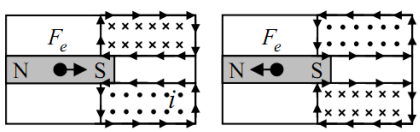

Figure 8: Electromagnetic induction

We investigated two properties, frequency and duty cycle, of the control input for use in the experiments. The optimized values for control input were obtained prior to the experiment. The capsule robot moved on the flat plane of a plastic plate and we measured its velocity using a high-speed camera. The optimized frequency was 35 Hz at positive amplitude +3 volts, negative amplitude −1 volt and duty cycle 50% for the control input. The fastest motion of the capsule robot was about 18 mm/s as shown in Figure 9. In addition, the optimized duty cycle was about 40–50% at positive amplitude +1 volt, negative amplitude −3 volts and frequency 35 Hz for the control input as shown in Figure 10. However, many parameters can affect the frequency and duty cycle of the control input, such as mass ratio between the body mass and inner mass, capsule robot size and stroke length. Hence, these optimized control input values were used only for this specific capsule robot.

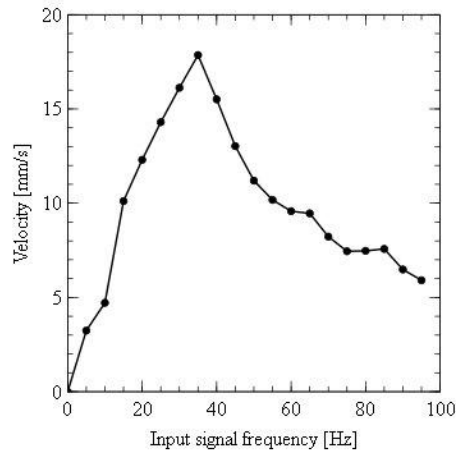

Figure 9: Relationship between velocity of the capsule robot and frequency of control input

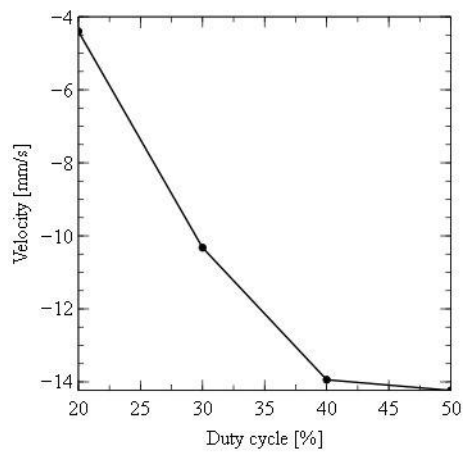

Figure 10: Relationship between velocity of the capsule robot and duty cycle of control input

4 Experiment

Two experiments were conducted. The objective of the first one was to determine the coefficient of static friction and that of the second one was to examine the displacement of the capsule robot motion.

4.1 *Coefficient of static friction experiment*

A simple experiment was set up to determine the coefficient of static friction as shown in Figure 11. The capsule robot moved on four types of material as shown in Figure 12. The capsule robot was placed on an inclined plane at the equilibrium state in Equation (16). When the angle was increased to a critical angle, the capsule robot started moving downwards. This critical angle is referred to as the coefficient of

static friction, and is given by Equation (17). The order from low to high values was plastic plate, sponge, sand paper and rubber, as shown in Table 2.

$$0 = Mg\sin\theta - \mu Mg\cos\theta \quad (16)$$

$$\mu = \tan\theta \quad (17)$$

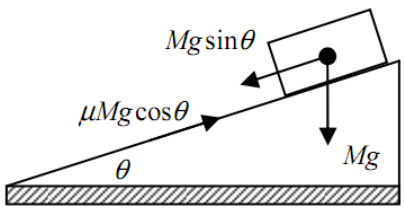

Figure 11: Free-body diagram of coefficient of static friction experiment

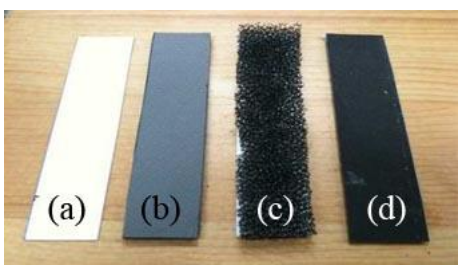

Figure 12: Materials for capsule robot motion: (a) plastic plate (b) rubber plate (c) sponge (d) sand paper

Table 2: Coefficient of static friction

Materials	μ
Plastic plate	0.23
Sponge	0.36
Sand paper	0.58
Rubber plate	1.00

4.2 *Capsule robot motion*

It was difficult to capture a video of the inner mass while it was moving because it was inside the body mass. Therefore, only a video of the body mass was captured. The capsule robot was set up on an inclined plane, which was adjusted to various angles. Power was supplied to the capsule robot by two small cables (source and ground) as shown in Figure 13(a). We used a high-speed (1000 f/s) camera to capture the capsule robot motion. Since the motion of the inner mass was not measured, the motion of the body mass was considered as the capsule robot motion.

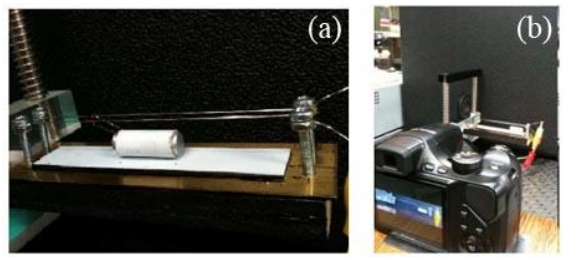

Figure 13: Capsule robot motion experiment setup: (a) capsule robot on inclined plane (b) camera position

The high-speed camera was set up in front of the inclined plane and parallel to the capsule robot motion as shown in Figure 13(b). After capturing the video, it was converted to a series of images, which were cropped to show only the capsule robot moving area. Binary images were obtained by thresholding. The grain noise was reduced by using a low-pass filter. The pixel positions of the capsule robot were identified at the center of the capsule robot by blob analysis[9]. Consequently, each pixel position of the capsule robot was converted to real displacement by multiplying by the pixel ratio (mm/pixel) as shown in Figure 14.

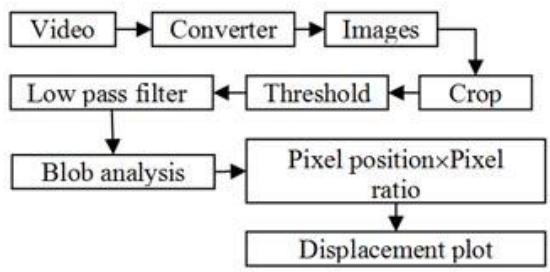

Figure 14: Diagram of process of measuring the capsule robot motion

We applied the image processing measurement method to the experiment, and found that the capsule robot motion graph in Figure 15 was similar to the characteristics graph of the body mass motion in Figure 4.

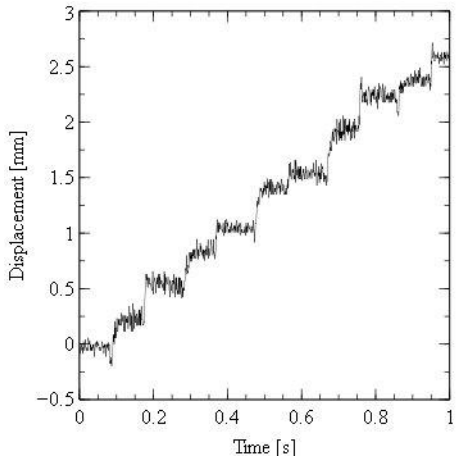

Figure 15: Motion of the capsule robot on plastic plate at the frequency of 5 Hz and $\theta = 0^{\circ}$

In the experiment, positive velocity corresponded to the capsule robot moving up the inclined plane and negative velocity down the inclined plane. The capsule robot moved upwards slowly while the angle of the inclined plane was increased. The order of average velocity from high to low was when the capsule robot moved upwards on the plastic plate, sponge, sand paper and rubber, as shown in Figure 16.

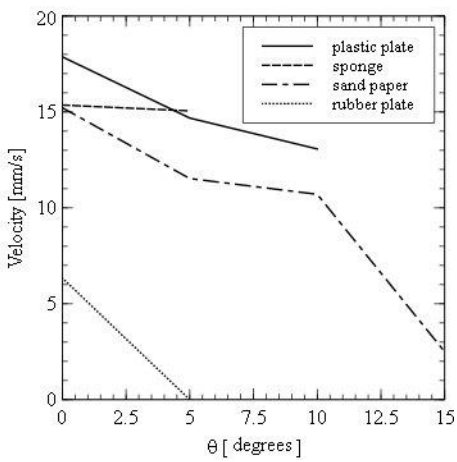

Figure 16: The capsule robot moved upwards on the inclined plane at positive amplitude +3 volts, negative amplitude −1 volt, frequency 35 Hz and duty cycle 50% of control input

The capsule robot moved downwards quickly when the angle of the inclined plane was large, as shown in Figure 17. The order of velocity from high to low when moving downwards was the same as that for moving upwards. The order of velocity for moving upwards and downwards was relative to the coefficient of static friction in Table 2. A low coefficient of static friction produced a low friction force as shown by Equation (3). Consequently, the capsule robot was able to move faster when the coefficient of static friction was lower.

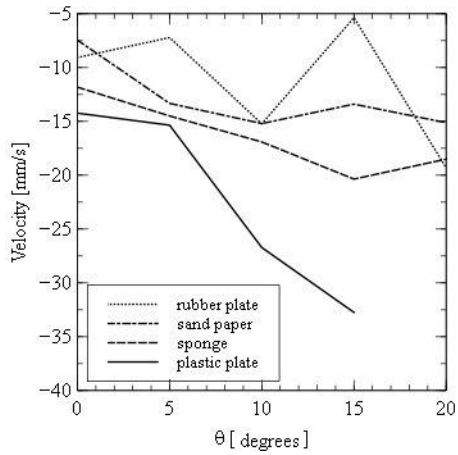

Figure 17: The capsule robot moved downwards on the inclined plane at positive amplitude +1 volt, negative amplitude −3 volts, frequency 35 Hz and duty cycle 50% of control input

5 Simulation

We prepared trend graphs using the system diagram according to Section 2. The parameters were as follows: $m_1 = 1.5\times10^{-4}$ Kg, $m_2 = 5.0\times10^{-5}$ kg, frequency 5 Hz, $\theta = 0^{\circ}$, $Gain = 3$ and $R = 1$. We then applied the input voltage U through MATLAB Simulink as shown in Figure 18. This caused changes in electrical current i , inductance of the coil L , electromagnetic force F_e and velocity of body mass $\dot{r}_1$ and inner mass $\dot{r}_2$, as shown in Figure (19) to (22). From the collision equation described in Equations (6) to (8), the inner mass had a high-stroke motion and moved faster than the body mass, as shown in Figure 23.

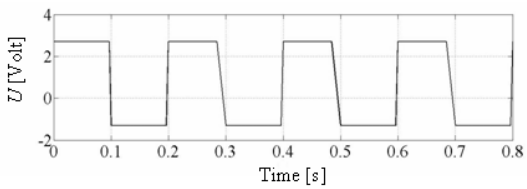

Figure 18: Voltage input

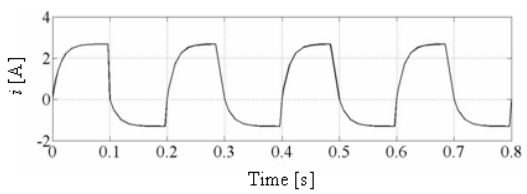

Figure 19: Electrical current

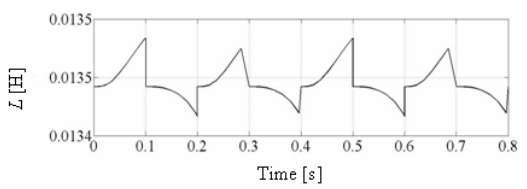

Figure 20: Inductance of the coil

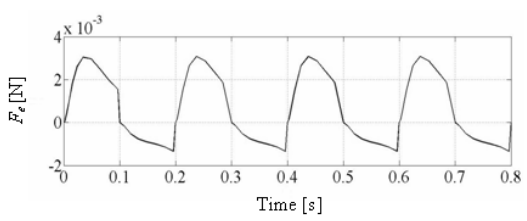

Figure 21: Electromagnetic force

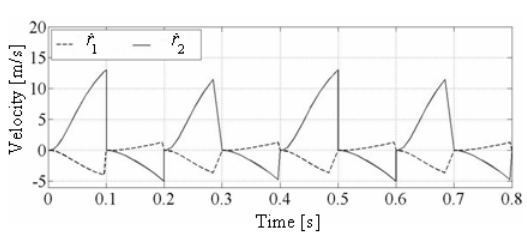

Figure 22: Velocity of body mass and inner mass

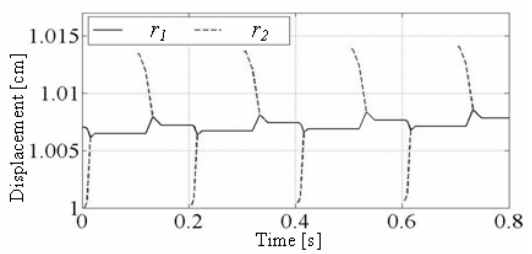

Figure 23: Displacement of body mass and inner mass

However, the friction force was greater than the electromagnetic force in several cases where the incline was steep and the capsule robot was unable to move. We therefore applied the appropriate electromagnetic force directly to the mechanical subsystem. The maximum and minimum electromagnetic force was +0.08 N and −0.02 N for moving up the incline, and +0.02 N and −0.08 N for moving down the incline at the frequency of 5 Hz. The results of simulation demonstrated that the upwards and downwards movement of the capsule robot simulation on the inclined plane had the same order of velocity from high to low as shown in Figure (24) and (25).

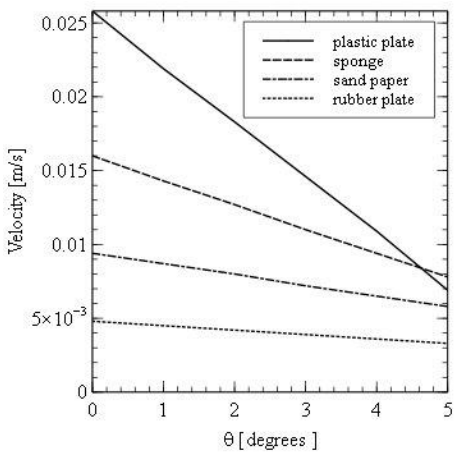

Figure 24: Relationship between velocity of upward-moving capsule robot and angle of inclined plane from simulation

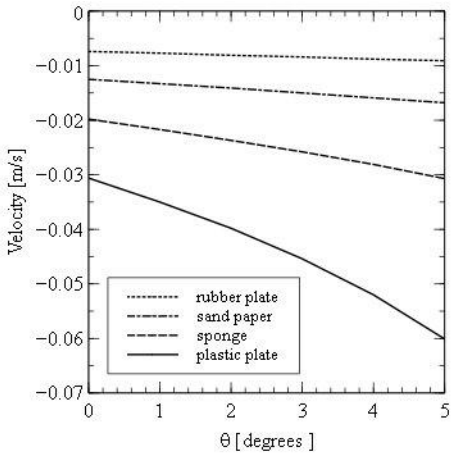

Figure 25: Relationship between velocity of downward-moving capsule robot and angle of inclined plane from simulation

The order of velocity was plastic plate, sponge, sand paper and rubber, which matched the simulation results. The change in velocity of the capsule robot was inversely proportional to the coefficient of static friction. In addition to numerical simulation, computer graphic simulation was also used to verify the equations of motion of the capsule robot as described in Section 2. The simulation tools were MATLAB (Virtual Reality Toolbox), VRML2.0, Cosmos Player VRML Plug-in and web browser (Netscape Communicator 4.5). The capsule robot motion was simulated by MATLAB programming and then displayed in the web browser as shown in Figure 26.

Figure 26: Computer graphic simulation

6 Conclusions

Although the capsule robot does not have a high-power actuator, it is able to move upwards on an inclined plane by inertia and friction forces under the constraints of a small angle of incline and low coefficient of static friction. Experiments demonstrated that the friction force between the capsule robot and the surface is not constant. In addition, other properties of the material should be considered, such as soft, rough and elastic properties. However, the coefficient of static friction can be used to predict the velocity of the capsule robot in a simple model of motion.

Future tasks include applying the capsule robot motion measurement method using a high-speed camera for feedback control and conducting an experiment on stimulating forces in a virtual intestinal environment.

Acknowledgments

This research was supported by a Grant-in-Aid for Scientific Research from the Japan Society for the Promotion of Science (#20560244).

References

[1] I. Wilding, P. Hirst, A. Connor, 2000. Development of a new engineering-based capsule for human drug absorption studies, Pharmaceutical Science and Technology Today, (3): 385–392.

[2] S.H. Woo, K.W. Yoon, Y.K. Moon et al., 2009. High Speed Receiver for Capsule Endoscope, Journal of Medical Systems, Springer Science, DOI 10.1007/s10916-009-9298-1.

[3] Y. Zhang, M. Yue, D. Guo, D. Wang, H. Yu, S. Jiang, X. Zhang, 2000. Characteristics of spatial magnetic torque of an intestine capsule micro robot with a variable diameter, Science in China Series E: Technological Sciences, (52): 2079–2086.

[4] P. Valdastri, R.J. Webster, C. Quaglia, M. Quirini, A. Menciassi, P. Dario, 2009. A New Mechanism for Meso-Scale Legged Locomotion in Compliant Tubular Environnents, IEEE Transactions on Robotics, (25): 1047–1057.

[5] A. Menciassi, S. Gorini, G. Pernorio, P. Dario, 2004. A SMA Actuated Artificial Earthworm,

ICRA, Robotics and Automation in Proceedings of IEEE International Conference, New Orleans, 3282–3287.

[6] Woo S. H., Kim T. W., Lee J. H., Kim P. U., Won C. H. and Cho J. H., 2009. Implemented edge shape of an electrical stimulus capsule, Int J Med Robotics Comput Assist Surg, (5): 59–65.

[7] T. Ito, S. Ishimori, T. Hayashi, 2010. Impulse-driven Micromechanism Capsule, Journal of Mechanical Design, System and Manufacturing, (4): 315–323.

[8] V. Giurgiutiu, S.E. Lyshevski, 2009. MICROMECHATRONICS Modeling, Analysis, and Design with MATLAB, second ed., CRC Press.

[9] R.C. Gonzalez, R.E. Woods, S.L. Eddins, 2003. Digital Image Processing Using Matlab, Prentice Hall.